ISBN: 978-3-95450-201-1 doi:10.18429/JACoW-IBIC2018-MOPA16

DESIGN OF A COMPACT PERMANENT MAGNET SPECTROMETER FOR CILEX/APOLLON

M. Khojoyan, A. Cauchois, J. Prudent, A. Specka
LLR (Laboratoire Leprince-Ringuet), CNRS and Ecole Polytechnique, Palaiseau UMR7638, France

Abstract

Laser Wakefield acceleration experiments make extensive use of small permanent magnets or magnet assemblies for analyzing and focusing electron beams produced in plasma accelerators. This choice is motivated by the ease of operation inside vacuum chambers, absence of power-supplies and feedthroughs, and potentially lower cost. Indeed, in these experiments space is at premium, and compactness is frequently required. At the same time, these magnets require a large angular acceptance for the divergent laser and electron beams which imposes constraint of the gap size. We will present the optimized design and characterization of a 100 mm long, 2.1 Tesla permanent magnet dipole. Furthermore, we will present the implementation of this magnet in a spectrometer that will measure the energy spectrum of electrons of ~ [60-2000] MeV with a few percent resolution in the CILEX/APOLLON 10PW laser facility in France.

INTRODUCTION

CILEX (Centre Interdisciplinaire de la Lumiere Extrême / Interdisciplinary Center for Extreme Light) is a research center which aims at using the Apollon-10P laser for exploring laser-matter interaction at extremely high laser intensities ($\sim 10^{22} W/cm^2$). The long focal length area of CILEX will be used to investigate plasma acceleration and radiation generation. It will be equipped with two interaction chambers able to accommodate laser focal lengths ranging from 3 m to 30 m. The spectrometer magnet presented here is designed to be compatible with the mentioned laser parameters.

A sketch of the laser-plasma interaction chamber is shown in Fig. 1. The total volume of interaction chamber is about $3m^3$ and it is practical to use permanent magnets for characterization of electron beam. Permanent magnets as compared to electromagnets, do not need power supplies (and consequently cooling system) and can be more compact due to smaller apertures. In our case, the apertures of the magnets will be limited by the laser envelope size, which according to our requirements, should pass through the magnets unobstructed. The paper is organized as follows. First, the design considerations of a permanent magnetic dipole are introduced together with analytical and computational field estimations. Next, construction of a permanent dipole magnet and magnetic field measurements are presented. Finally, beam dynamics simulation results are obtained by applying the magnet as a spectrometer inside the interaction chamber of the CILEX facility.

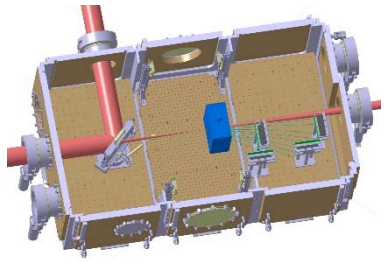

Figure 1: Schematic of interaction chamber at CILEX with laser envelope shown in red and magnetic dipole shown in blue. Measurement screens and reference electron trajectories are shown as well.

Let us consider a simple C shaped dipole (Fig. 2). The field in the gap of height h_g is driven by a permanent magnet of the same height $h_{pm} = h_g$ and of width w_{pm}.

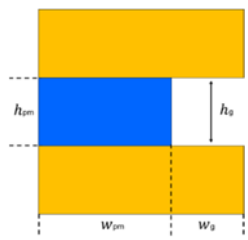

Figure 2: 2D view of a C shaped dipole with a permanent magnet shown in blue and steel/iron in yellow colors.

Assuming constant field in the gap (no horizontal field component) it is straightforward to calculate the magnetic flux density using Ampere's and flux conservation laws:

$$B_g = -\frac{B_r w_{pm}}{w_g + \frac{\mu_r h_g w_{pm}}{h_{pm}}} \quad (1)$$

with B_r and μ_r being the remnant field and relative permeability of the permanent magnet. From Eq. 1 it follows that the maximum achievable field in the gap cannot exceed the remnant induction field of the magnet independent of how small the gap width (w_g) and how large the magnet width (w_{pm}) are. It becomes clear that for a permanent magnet (PM) dipole, to reach fields higher than remnant field of an individual magnet, a special arrangement of magnetic sub-materials is necessary. Common structures are Halbach [1] and Stelter [2] configurations. In [3] a cylindrical structure was originally proposed by Halbach and

ISBN: 978-3-95450-201-1 doi:10.18429/JACoW-IBIC2018-MOPA16

has later on been improved [4] by using iron poles inside the structure. A spherical structure was introduced in [5] and was later improved by using FeCo material as a pole piece [6]. Nowadays, permanent magnet dipoles are widely used in magnetic resonance imaging applications [7], in facilities such as third [8-10] and next [11, 12] generation light sources. Neodymium iron Boron (Nd-Fe-B) magnets are the preferred candidates for generating strong magnetic fields due to their high remnant induction and the highest up to date BH energy product [13, 14]. Moreover, almost linear behaviour of the demagnetization curve [3] and relative permeability close to unity makes the analytical design of such systems relatively straight forward.

DESIGN OF A PM DIPOLE: ANALYTIC ESTIMATION OF MAGNETIC FIELD

For design considerations of a magnetic dipole we assume that the magnet is H shaped with a 2D schematic view (upper half) shown in Fig. 3. The parts shown in yellow color represent iron material: pole tip as well as the yokes for the flux circulation. The pole tip is surrounded by neodymium iron boron magnets with arrows indicating magnetization direction of each magnet. In the same scheme h_g is half the gap height and w / h signify the width / height of each surrounding magnet. The main idea of using such geometry is the collection of the flux from the surrounding permanent magnets and concentration into the magnet gap. The strength of the magnet built in this way can therefore exceed the residual field (B_r) of the permanent magnet materials and, in principle, reach the saturation field of pole material which can be more than 2 Tesla. Next, applying flux conservation and Ampere's laws [15] for the above magnetic circuit (and neglecting fringe field effects), one can obtain the following expression for magnetic flux density in the gap:

$$B_g = -\frac{1}{h_g}\frac{\left(w_1 + w_2 + w_3\right)B_r}{\left(\frac{w_g}{h_g} + \frac{\mu_r w_1}{h_1} + \frac{\mu_r w_2}{h_2} + \frac{\mu_r w_3}{h_3}\right)} \quad (2)$$

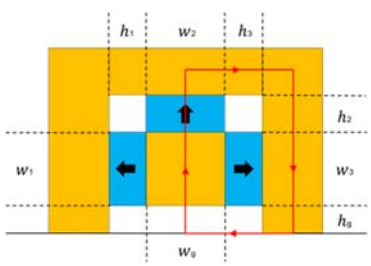

Figure 3. Schematic (2D) view of top half of H shaped magnet with a red flux line following Ampere's law. Iron is shown in yellow with the pole tip surrounded by Neodymium N40 grade magnets expressed in light blue.

It is possible to further optimize the latter expression assuming a square shape magnet poles and surrounding magnets of similar sizes. Since the gain in magnetic field over magnet weight is an important measure on designing a magnet, Fig. 4 illustrates the total weight of the surrounding magnets and the peak magnetic field as function of polesize for a gap height of 10 mm. Note that the weight does not increase linearly with the pole size. In practice, the pole dimensions are chosen according to the needs of transverse good field region required from beam dynamics. In our case the pole size of 51 mm was rather chosen according to the sizes of Nd-Fe-B 40 grade magnets commercially available in the market.

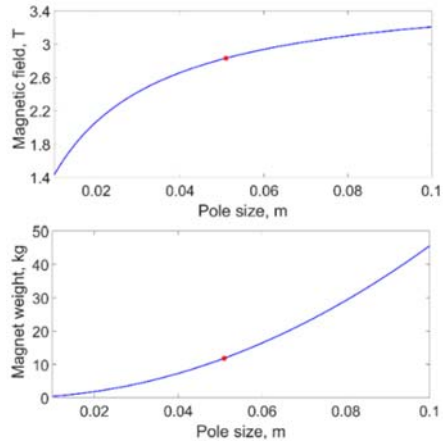

Figure 4: Total weight of magnets and peak magnetic field as function of pole size. Red asterisks represent the corresponding expected values for 51 mm magnet pole size. 10 mm gap size/height is assumed in the plot.

DESIGN OF A PM DIPOLE: COMPUTATION OF MAGNETIC FIELD

The magnet geometry of Fig. 3 has been studied using three-dimensional TOSCA software [16]. Following dimensions have been used in the calculations: $h_1 = h_3 = 5.08cm$, $w_1 = w_3 = 7.08cm$, $h_2 = w_2 = 5.08cm$. For the case of neodymium magnet, by taking advantage of linear BH behaviour in the second quadrant of BH curve, the slope μ_r is calculated depending on the grade of the magnet. Non-linear iron properties have been used in TOSCA for induction versus field data. The aim was to reach magnetic field at the gap as close as possible to the saturation field of the pole material. A fixed ratio of 20 for magnet gap height over length was imposed. Figure 5 illustrates the expected peak magnetic flux density at the magnet gap for different gap heights obtained from TOSCA simulations (red circles) assuming 2.26 T saturation field for the iron. In the same plot analytical estimation of the field is shown applying an empirical scale factor 2.26 / 2.96, where 2.96 T corresponds to the analytical peak field value for 10 mm gap allowing infinitely high saturation field for the iron. It can be seen from the plot that for the case of 10 mm gap, the value of peak magnetic field in the gap is close to the saturation field of the iron and, in the same time, for larger gap sizes the considered geometry is not optimum anymore.

ISBN: 978-3-95450-201-1 doi:10.18429/JACoW-IBIC2018-MOPA16

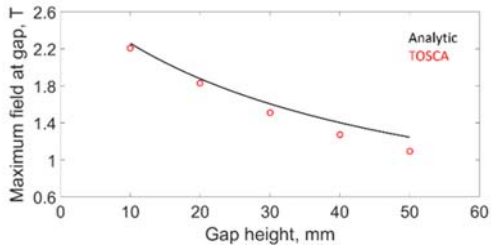

Figure 5: Magnetic induction in the gap for various gap sizes. Red dots: TOSCA calculations. Black curve: analytical estimation applying a factor 0.7635.

DESIGN OF A PM DIPOLE: CONSTRUCTION AND MEASUREMENTS

The PM dipole has been constructed at LLR (Laboratoire Leprince-Ringuet) using Nd-Fe-B 40 grade magnets as surrounding magnet material and allied pure iron (2.18 T saturation field) as pole and yoke material. A dedicated mechanical tooling and careful adjustment were the key points during the magnet assembly due to strong force existent between the magnets and corrosion risks that are not negligible for neodymium magnets. Furthermore, special arrangement of 56 magnets was needed during the assembly to balance the field imperfections of individual magnets (Fig. 6). In this plot the dimensions (w x h x l) of the magnets are shown in legends. However, it is believed, that geometry with iron poles will smoothen the effects of field imperfections and defects in the magnet once the iron is saturated. The assembled dipole and corresponding TOSCA model of the magnet are presented in Fig. 7. Magnets shown in blue have been added to strengthen the flux on both sides of iron poles. The magnetic length of the dipole was 100 mm. Finally, the assembled magnet was measured at the measurement bench of LLR laboratory.

The position of the Hall probe was aligned to the magnet using an optical system with high magnification camera (50 µm pixel resolution) in the field of view of 5 cm diameter centered on the pole gap at the magnet exit face (Fig. 8). The Hall probe was mounted on linear translation stages which, according to the manufacturer, have 0.07 microradians angular slope and 2 micrometers bidirectional repeatability [17]. Measured and simulated field profiles are summarized in Fig. 9. The result is remarkable yielding to less than 1 % disagreement between predicted and measured field values. No field weakening has been observed as a result of demagnetization effects [18] due to a very strong field at the specific corners of individual magnets (see TOSCA simulation of the magnet on the right side of the Fig. 7).

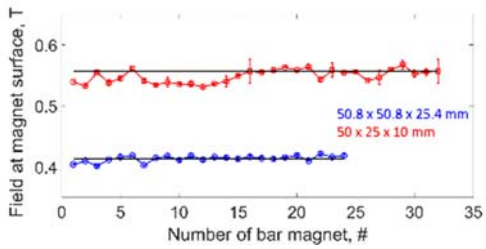

Figure 6: Measured magnetic induction at the surface of two types of neodymium magnets. For each case, black lines represent analytically estimated field value assuming 0.5 mm offset of Hall probe sensor from the magnet surface.

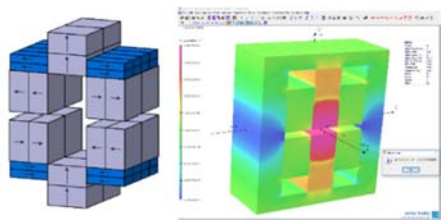

Figure 7: Left: overview of different block magnets used to assembly the dipole. Arrows on the blocks illustrate the magnetization directions. Right: TOSCA model of magnet yielding 2.092 T peak field value in the gap. The main component of induction field is shown in color map from blue (lowest value) to red (highest value).

Figure 8: Left: LLR measurement bench with a Hall probe mounted on linear transition stages. Right: defined area of interest for hall probe alignment using optical system.

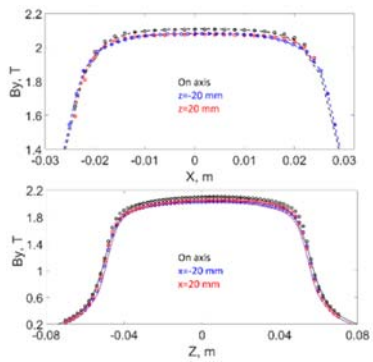

Figure 9: On and off-axis main component field profiles along horizontal (upper plot) and longitudinal (lower plot) directions. For each case dots correspond to the measured and curves to the simulated field values. A scaling factor (~ 1 %) is applied to match the measured and simulated field values.

ISBN: 978-3-95450-201-1 doi:10.18429/JACoW-IBIC2018-MOPA16

IMPLEMENTATIN OF PM DIPOLE AS A SPECTROMETER

ASTRA [19] simulation software has been applied to study the dynamics of different energy electrons through the designed magnet. The considered electron energy range of 56-2350 MeV has been defined as the lowest energy exiting the magnet from the side of the mechanical gap and the highest energy which is measurable out of 50 mrad divergent laser cone. An idealized electron bunch having Gaussian distribution in all sub spaces was assumed in simulations. Electron beam parameters are summarized in Table 1. 3D magnetic field map has been implemented into ASTRA for the correct treatment of fringe field effects. Electron reference trajectories of different energies and corresponding screens (marked as S#) are illustrated in Fig. 10. In the same figure, the mid plane magnetic field profile is shown in color map.

Table 1: Electron Beam Parameters used in ASTRA.

LPA beam parameter	Value
Charge, pC	10
Energy, MeV	56-2350
Transverse rms size, μm	2.5
Transverse rms divergence, mrad	2

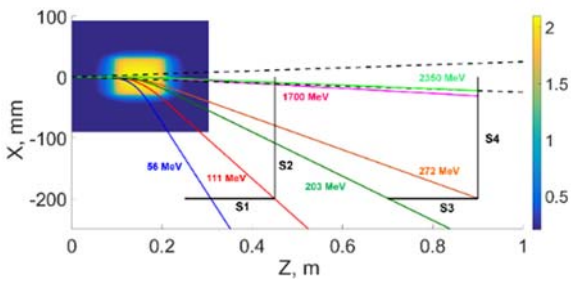

Figure 10: Range of electron trajectories and corresponding screen positions/orientations for energy measurement inside the interaction chamber of CILEX.

Horizontal displacement obtained from the simulated trajectories concedes very well with a simple geometrical estimation (assuming hard edge magnetic field profile) once the electrons exit on the side of the magnet (see Fig. 11). Figure 12 plots the beam envelopes at the positions of S1 and S2. In the plot the black line indicates the separation of the screens. Electrons of energies below 200 MeV are strongly affected by the fringe field focusing effects. In addition, the fringe field effects may be further enhanced / diminished by adjusting the magnet laterally. The rms energy resolution at various screens and at different energies is plotted in Fig. 13 which yields less than 8 % rms value within the whole energy range for 2 milliradians divergence of electron beam.

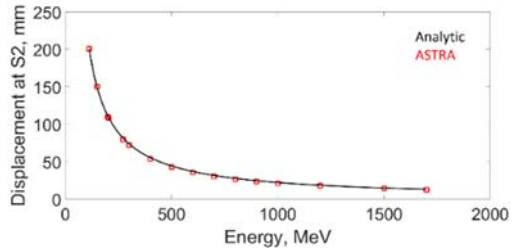

Figure 11: Horizontal displacement at the position of S2. Black curve: analytical estimation, red circles: ASTRA.

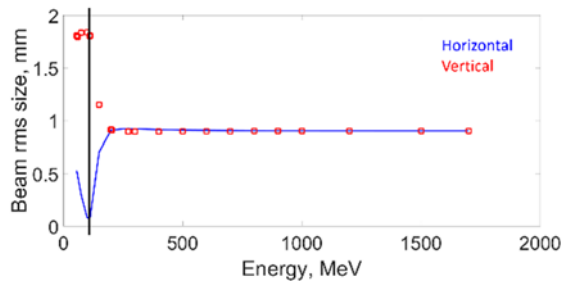

Figure 12: Beam rms transverse sizes at screen positions of S1 and S2. Blue line: horizontal, red rectangles: vertical.

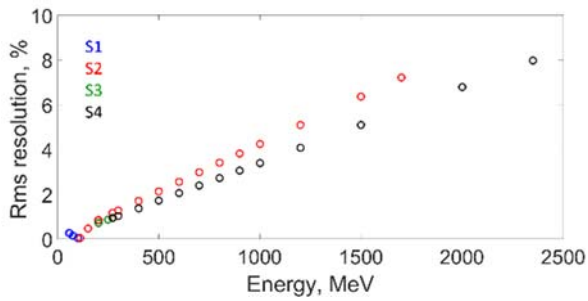

Figure 13: rms energy resolution estimated at different screens for 2 milliradians electron beam divergence. Different colors symbolize the outcome at different screen positions.

SUMMARY

A 2.1 Tesla permanent magnet dipole has been designed, constructed, measured and characterized as a spectrometer for CILEX. Very good agreement (~ 1 %) between predicted and measured magnetic field values has been obtained. A precise electron beam tracking has been done afterwards by applying the 3D field map of the magnet into ASTRA simulation program. According to tracking results the magnet will enable to measure electrons from 56 MeV to 2.35 GeV with rms resolution of below 10 percent at full energy range. Besides, for smaller laser divergence the magnet can be shifted downstream and the energy resolution may be improved by adding a focusing element into the configuration.

ACKNOWLEDGEMENTS

The work is partially supported by the European Union's Horizon 2020 Research and innovation programme under grant agreement No 730871.

ISBN: 978-3-95450-201-1 doi:10.18429/JACoW-IBIC2018-MOPA16

REFERENCES

[1] K. Halbach, "Application of permanent magnets in accelerators and electron storage rings", *Journal of Applied Physics* vol. 57, p. 3605, 1985.

[2] R. E. Stelter, "Dipole permanent magnet structure", United States patent, 1997.

[3] K. Halbach, "Design of permanent multipole magnets with oriented rare earth cobalt material", *Nuclear Instruments and Methods*, vol. 169, pp. 1-10, 1980.

[4] M. Kumada *et al.*, "Development of 4 Tesla permanent magnet", in *Proc. PAC'01,* Chicago, IL, USA, Jun. 2001, pp. 3221-3223.

[5] H.A. Leupold and E. Potenziani, "Novel high-field permanent-magnet flux sources", *IEEE Transactions on Magnetics*, vol. 23, no. 5, pp. 3628-3629,1987.

[6] F. Bloch, O. Cugat, G. Meunier, and J. C. Toussaint, "Innovating approaches to the generation of intense magnetic fields: Design and optimization of a 4 Tesla permanent magnet flux source", *IEEE Transactions on Magnetics*, vol. 34, no. 5, pp. 2465-2468, 1998.

[7] C. Li and M. Devine, "Efficiency of permanent magnet assemblies for MRI devices", *IEEE Transactions on Magnetics*, vol. 41, no. 10, pp. 3835-3837, 2005.

[8] J.M. Ortega *et al.*, "Optimization of a permanent magnet undulator for free electron laser studies on the ACO storage ring", *Journal of Applied Physics*, vol. 54, p. 4776, 1983.

[9] G. Tosin, R. Basílio, S. Casas, and R. J. F. Marcondes "Bending magnets made with permanent magnets for LNLS-2 electron storage ring", in *Proc. PAC'09*, Vancouver, BC, Canada, May 2009, paper MO6PFP001, pp. 127-129.

[10] E. Nakamura, K. Egawa, K. Takayama, and K. Ogata, "Permanent magnets for the 500 MeV accumulator ring of the intensity doubler project in KEK-PS", in *Proc. 18th Int. Conf. on High-Energy Accelerators (HEACC 2001),* Tsukuba, Japan, Mar. 2001, paper P2oth11.

[11] T. Watanabe *et al.*, "Permanent magnet based dipole magnets for next generation light sources*", Physical Review Accelerators and Beams,* vol. 20, p. 072401, 2017.

[12] S.C. Gottschalk *et al.*, "Permanent magnet systems for free-electron lasers", *Nuclear Instruments and Methods in Physics Research A*, vol. 507, pp. 181-185, 2003.

[13] J.F. Herbst *et al.*, "Structural and magnetic properties of Nd2Fe14B", *J. Appl. Phys.,* vol. 57, p. 4086, 1985.

[14] D. Brown *et al.*, "Developments in the processing and properties of NdFeB-type magnets", *Journal of Magnetism and Magnetic Materials*, vol. 248, pp. 432-440, 2002.

[15] B. C. Brown, "Design formulas for the strength, compensation and trimming of hybrid permanent magnets", Fermilab, Batavia, IL, USA, Rep. FERMILAB-Conf-96/273, 1996.

[16] TOSCA, Opera-3d, Cobham Technical Services, http://operafea.com/, Software for electromagnetic design, Oxford, UK.

[17] Thorlabs: Linear Translation Stages, see for example in: https://www.thorlabs.com/newgrouppage9.cfm?objectgroup_id=7652

[18] M. Katter, "Angular dependence of the demagnetization stability of sintered Nd-Fe-B magnets", *IEEE Transections on Magnetics*, vol. 41, no. 10, pp. 2853-3855, 2005.

[19] K. Floettmann, ASTRA, http:/www.desy.de/mpyflo